Schweizerischer Erdbebendienst
Service Sismologique Suisse
Servizio Sismico Svizzero
Swiss Seismological Service

ETH zürich

# SITE CHARACTERIZATION REPORT

# SBAK: Basel (BS) - Klybeck

Manuel Hobiger, Clotaire Michel, Donat Fäh

Last Modification: 25/02/2020

Schweizerischer Erdbebendienst (SED)
Service Sismologique Suisse
Servizio Sismico Svizzero
Servizi da Terratrembels Svizzer

ETH Zürich
Sonneggstrasse 5
8092 Zürich
Schweiz
manuel.hobiger@sed.ethz.ch

# Contents

# Summary

The free-field strong-motion station SBAK was built next to the Schulhaus Horburg in Basel-Klybeck (BS). We performed a passive seismic array measurement with two array configurations to characterize the soil underneath the station.
The measurements show that the fundamental frequency of the structure beneath the station is about 0.7 Hz. The array measurements were analyzed with different techniques, namely 3-component HRFK, WaveDec and SPAC. All techniques gave similar dispersion curves. The dispersion curves for the fundamental modes of both Love and Rayleigh waves could be retrieved from around 2 to over 20 Hz.
Similar to other places in Basel, it was not possible to successfully invert Love and Rayleigh waves together and the Love waves were therefore neglected in the inversion. The joint inversion of Rayleigh wave dispersion and ellipticity curves showed that the structure can be mainly explained by models with interfaces at around 20-25 m, 60-80 m and 230 m depth. The $V_{S30}$ of the best models is about 412 m/s, corresponding to soil class B in EC8 and C in SIA261.

# 1 Introduction

In the framework of the second phase of the Swiss Strong Motion Network (SSMNet) renewal project, a new station was planned in Basel-Klybeck (BS).
The site selection resulted in the Schulhaus Horburg as the best site in the area. The new station, called SBAK, went operational on 4 November 2014. The location of the station is shown in Fig. 1.

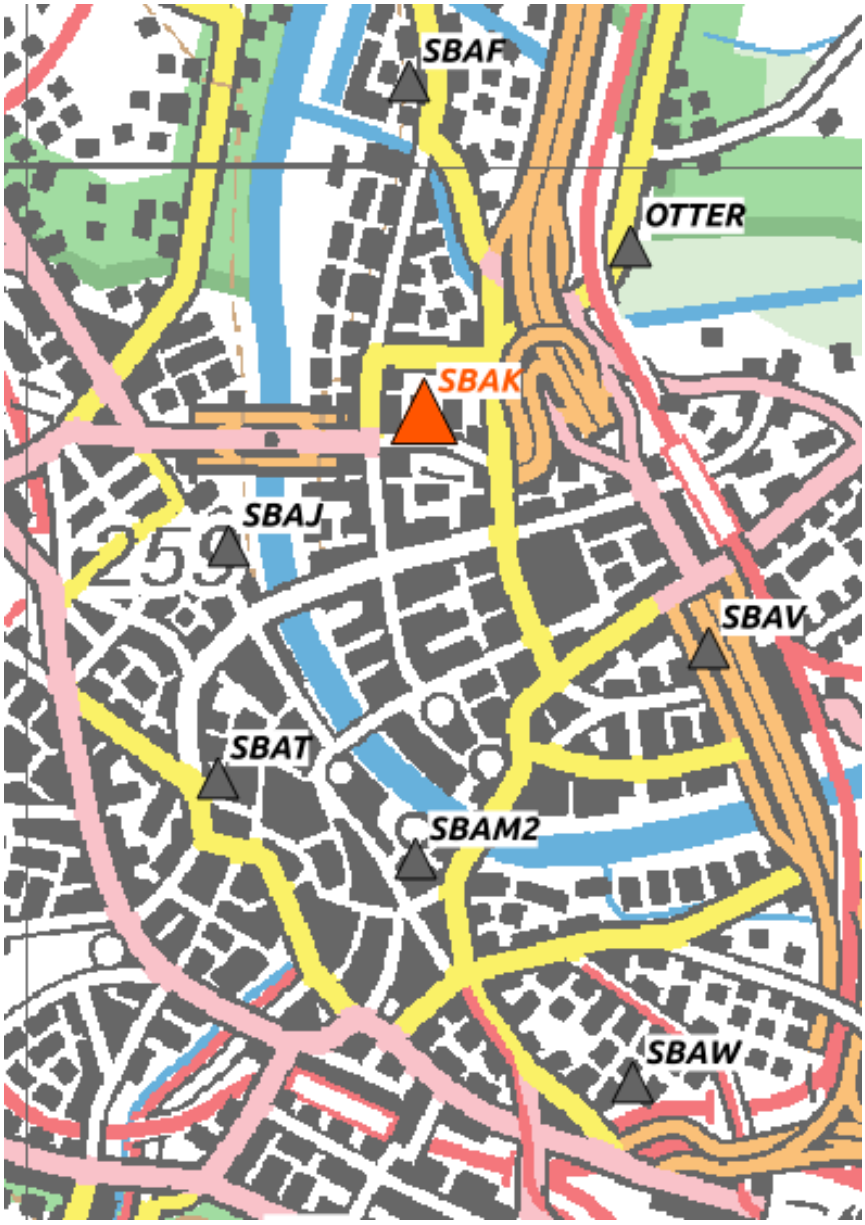


Figure 1: Map showing the location of station SBAK in Basel-Klybeck, together with other stations of the Swiss Strong Motion Network in Basel.

# 2 Geological setting

A geological map of the surroundings of station SBAK is shown in Fig. 2. The station is located on alluvial deposits of the Rhine.

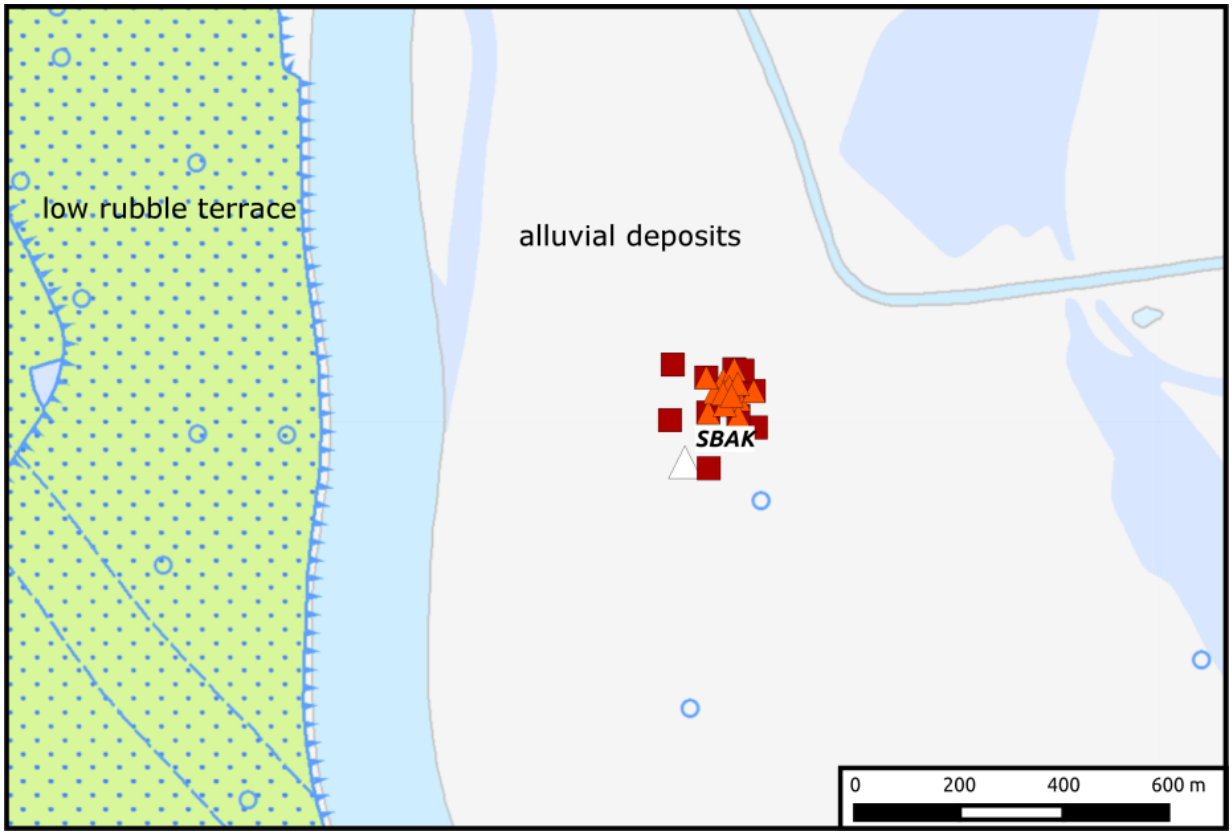


Figure 2: Geological map of the area around station SBAK. According to the geological atlas, station SBAK and all stations of the passive array measurement lie on alluvial deposits.

# 3 Site characterization measurements

## 3.1 Data set

In order to characterize the local underground structure around station SBAK, passive seismic array measurements were carried out on 24 October 2014. The layout of the seismic measurements is shown in Fig. 3.
Two array measurements were performed (see Table 1 for the main characteristics). The first array consisted of 14 stations, which were placed in the Horburg park. It was planned to consist of three rings, of which the central one should have a radius of 10 m and contain three stations. The second and third ring were planned to consist of five stations each and have radii of 25 m and 50 m, respectively. The final minimum and maximum inter-station distances in the first array were 9.9 m and 96.8 m, respectively. The names of the stations of the first array are composed of "SBAK" followed by a two-digit number between 01 and 14. The seismic stations consisted of Lennartz 3C 5 s sensors connected to Quanterra Q330 digitizers. A total of 12 digitizers were used, two sensors were connected to the same digitizer in some cases.
The second array consisted of 12 stations. For this array, the five stations located on the second ring were moved to outer positions in order to be located on a ring of radius 100 m. The center of this ring was shifted by 42 m to the south-west with respect to the center of the first array. One station of the innermost ring and the central station of the first array were kept in place during the second array measurement. The minimum and maximum inter-station distances of the second array were 10.0 and 210.4 m, respectively. The station names of the stations which were the same as in array 1 were kept, the moved stations got names composed of "SBAK" and a two-digit number between 21 and 31. The station locations have been measured by a differential GPS system (Leica Viva GS10) which was set up to measure with a precision better than 5 cm. This precision was achieved for most stations. For stations SBAK07, SBAK08 and SBAK12, the obtained precision was 6.3 cm, 13.7 cm and 16.1 cm, respectively. For stations SBAK25 and SBAK31, precisions of 23.5 cm and 44.6 cm were obtained. At these stations, trees deteriorated the GPS signals.

Table 1: List of the passive seismic array measurements in Basel-Klybeck.

| Array name | Number of sensors | Minimum interstation distance [m] | Maximum interstation distance [m] | Recording time [s] |
|---|---|---|---|---|
| 1 | 14 | 9.9 | 96.8 | 6300 |
| 2 | 12 | 10.0 | 210.4 | 8100 |

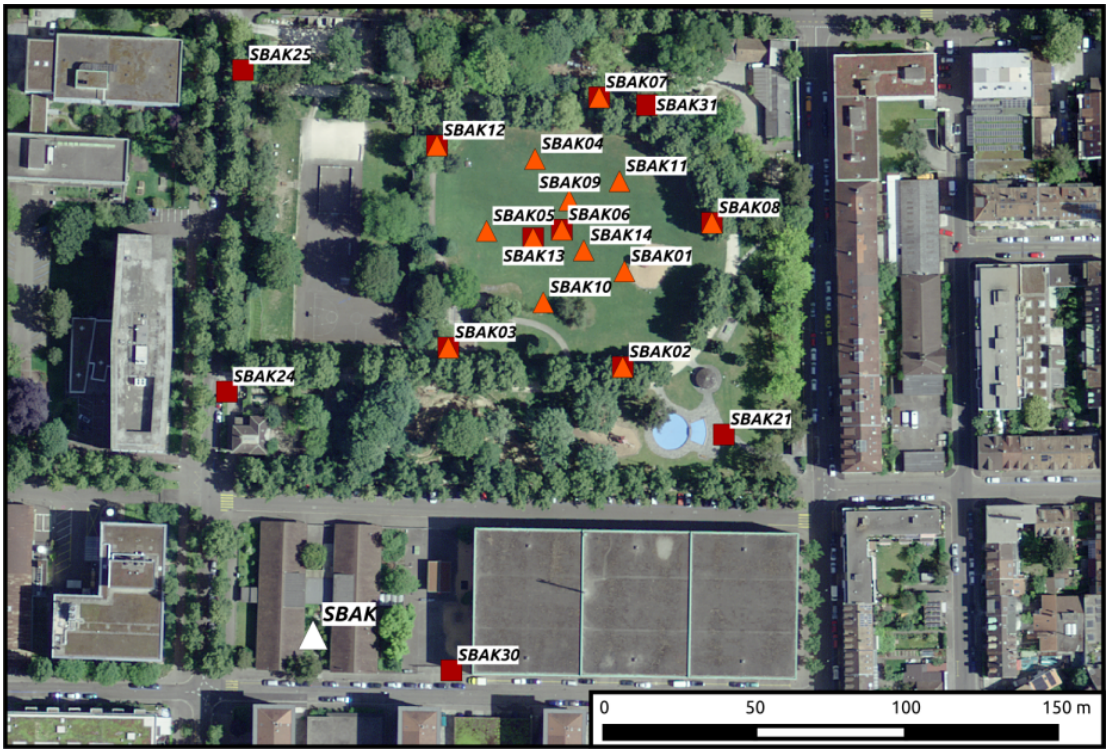


Figure 3: Layout of the array measurements around station SBAK. The location of SBAK is indicated by the white triangle, the locations of the stations for the passive seismic measurement by the orange triangles (first array) and red squares (second array). ©2019 swisstopo (JD100042)

## 3.2 H/V and RayDec ellipticity curves

Figure 4 shows the H/V curves determined with the time-frequency analysis method (Fäh et al., 2009) for all stations of both passive arrays. All curves are very similar and only show major differences above 5 Hz. The fundamental peak frequency at the different stations varies between 0.65 and 0.84 Hz.
The RayDec technique (Hobiger et al., 2009) is supposed to eliminate the contributions of other wave types than Rayleigh waves and give a better estimate of the ellipticity than the classical H/V technique. The RayDec ellipticity curves for all stations of the array measurements are shown in Fig. 4. Station SBAK06, the central station of array 1, serves as a reference and will be used for the inversion.
The RayDec curves are similar to the H/V curves, but the plateau around the fundamental peak is more flat.

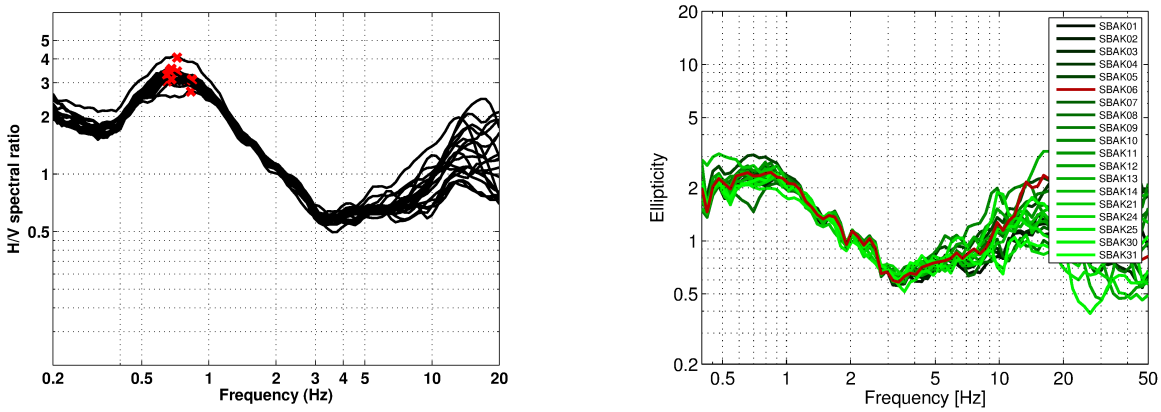


Figure 4: Left: Overview of the H/V measurements for the different stations of both array measurements. Right: RayDec ellipticities for all measurement stations.

## 3.3 Polarization measurements

The polarization analysis was performed according to Burjánek et al. (2010) and Burjánek et al. (2012). The results for all stations of the array are similar. Only the results for SBAK06, the station in the array center, are shown here.
There is no preferential linear particle polarization visible and we do not see indications for 2-dimensional polarization effects.

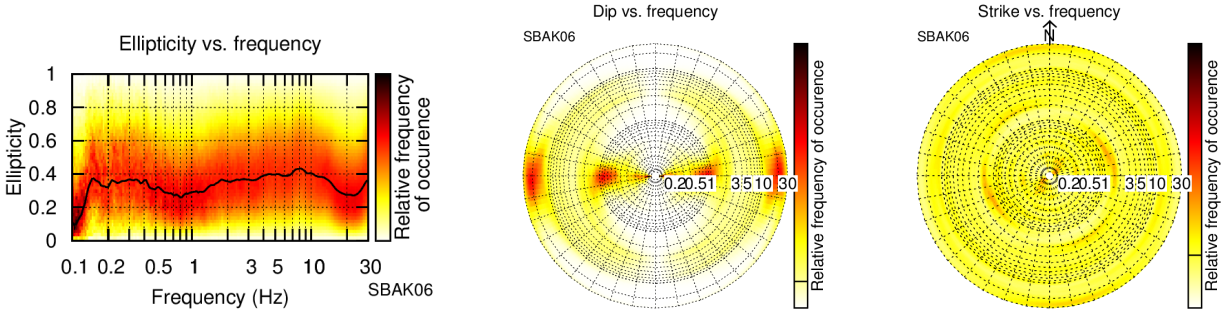


Figure 5: Polarization analysis of station SBAK06.

## 3.4 3-component high-resolution FK

The results of the 3-component high-resolution FK analysis (Poggi and Fäh, 2010) are shown in Fig. 6 (dispersion curves) and Fig. 7 (ellipticity curves). On the transverse component, corresponding to Love waves, we can clearly identify a dispersion curve for array 1 between 3.7 and 22.0 Hz and for array 2 between 2.0 and 9.5 Hz. The upper-frequency resolution limit of array 1 is not reached, some hints for higher modes are visible for array 1 above 15 Hz, but they were not picked.
On the vertical component, corresponding to Rayleigh waves, we can clearly identify one mode between 3.2 and 28.6 Hz for array 1 and between 2.0 and 7.7 Hz for array 2. A small portion of a dispersion curve of a higher mode is also visible between 16.9 and 23.5 Hz for array 1. On the radial component, also related with Rayleigh waves, we can also see dispersion curves for a single mode using each array.
The corresponding ellipticity curves of these modes (Fig. 7) do not show very pronounced peaks and troughs.

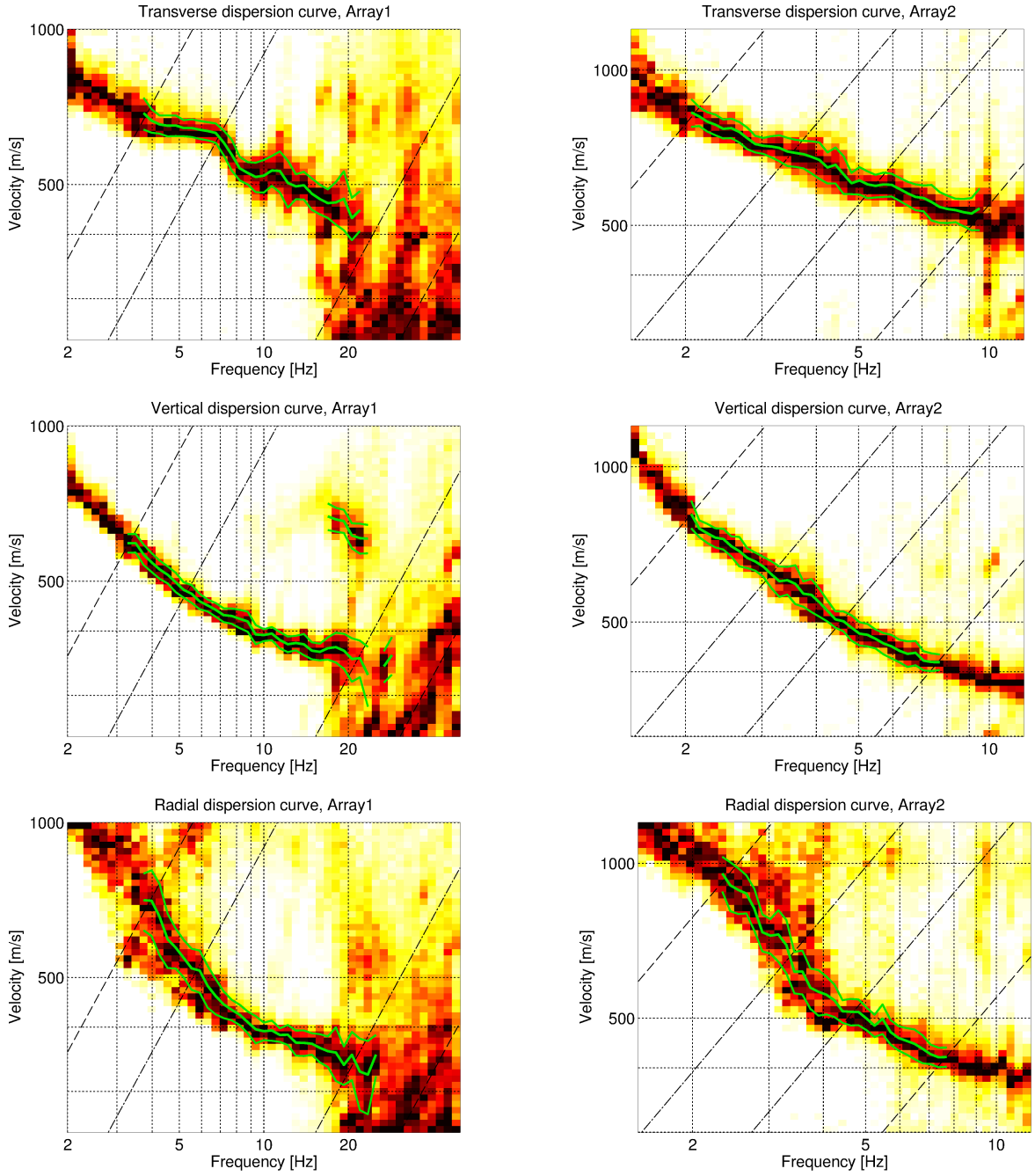


Figure 6: Dispersion curves obtained with the 3-component HRFK algorithm (Poggi and Fäh, 2010). In the left column, the dispersion curves for the transverse, vertical and radial components are shown for array 1, and in the right column for array 2. The dashed and dotted black lines are the array resolution limits. The solid green lines are picked from the data, where the central line indicates the best values and the two outer lines the standard deviation.

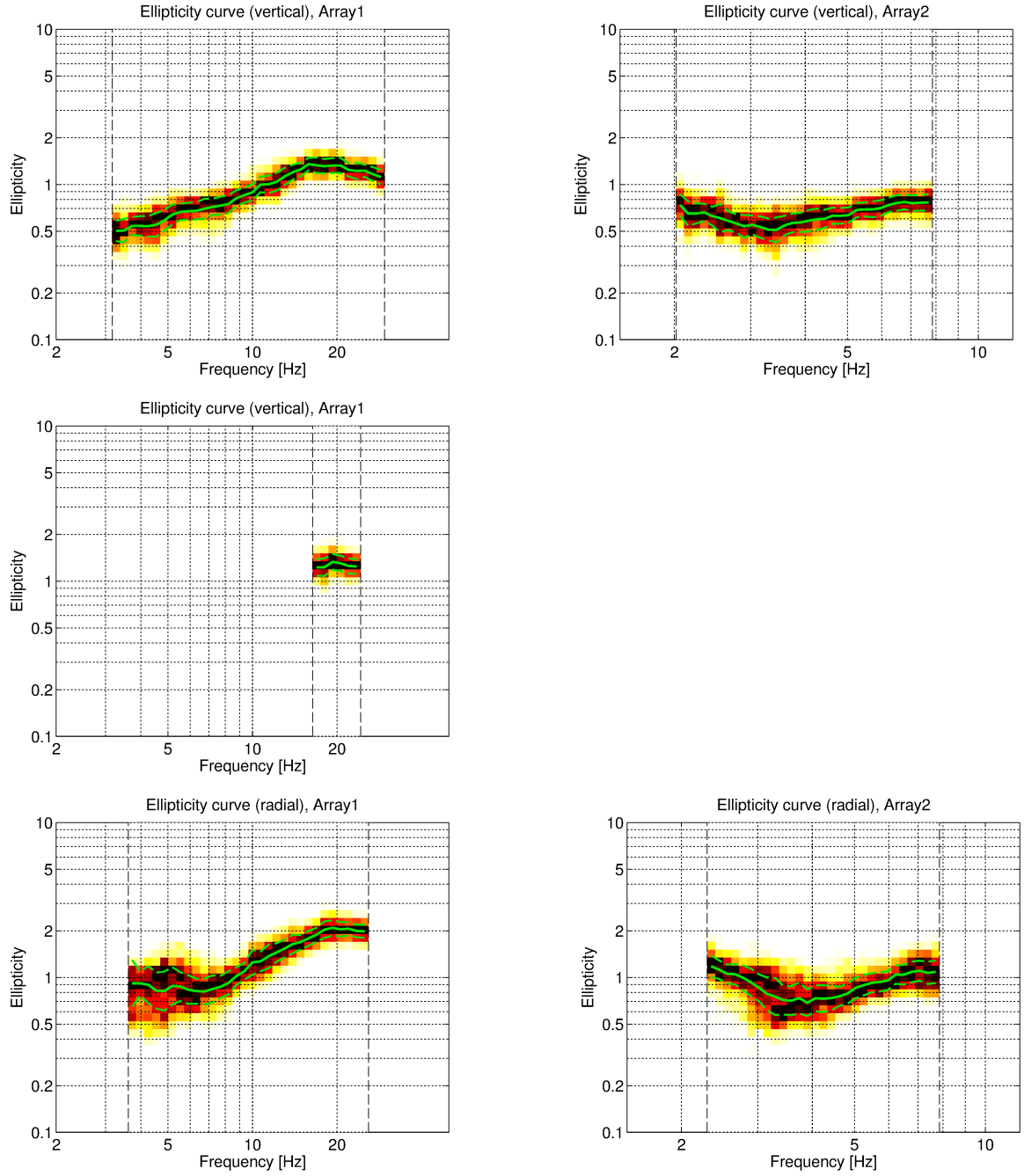


Figure 7: Ellipticity curves obtained with the 3-component HRFK algorithm (Poggi and Fäh, 2010) corresponding to the picked dispersion curves on the vertical and radial components for array 1 (left column) and array 2 (right column). The solid green lines are picked from the data, where the central line indicates the best values and the two outer lines the standard deviation.

## 3.5 WaveDec

The results of the WaveDec (Maranò et al., 2012) processing are shown in Figs 8 and 9. This technique estimates the properties of single or multiple waves simultaneously with a maximum likelihood approach. In order to get good results, the parameter $\gamma$, which modifies the sharpness of the wave property estimation, has been tuned. Here, a value of $\gamma = 0.2$ was used, corresponding to a mainly maximum likelihood estimation.
The Love wave dispersion curve is clearly identified, but with less precision than with 3-C HRFK, and was picked between 3.7 and 14.9 Hz for array 1 and between 2.3 and 8.1 Hz for array 2. Also here, the higher resolution limit of the array was not reached with array 1.
The Rayleigh wave dispersion curve is more smooth and picked between 3.4 and 19.3 Hz for array 1 and between 2.4 and 6.5 Hz for array 2. The ellipticity angle for the picked Rayleigh wave dispersion curves are always negative, indicating retrograde particle motion, but we see an indication of a change of the sense of rotation at around 20 Hz at the upper frequency limit of the picked curve.

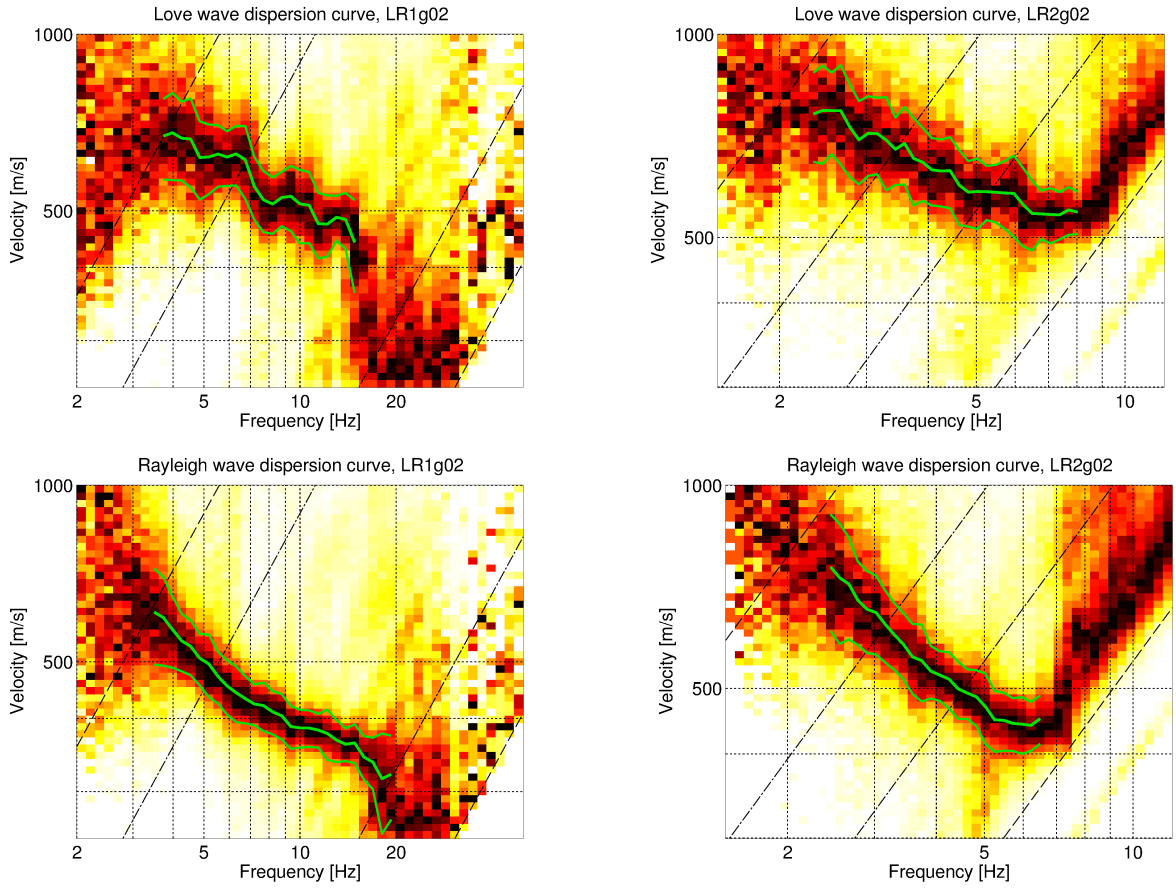


Figure 8: Love (top line) and Rayleigh (bottom line) wave dispersion curves obtained with the WaveDec technique (Maranò et al., 2012) for array 1 (left) and array 2 (right). The dashed lines indicate the theoretical array resolution limits.

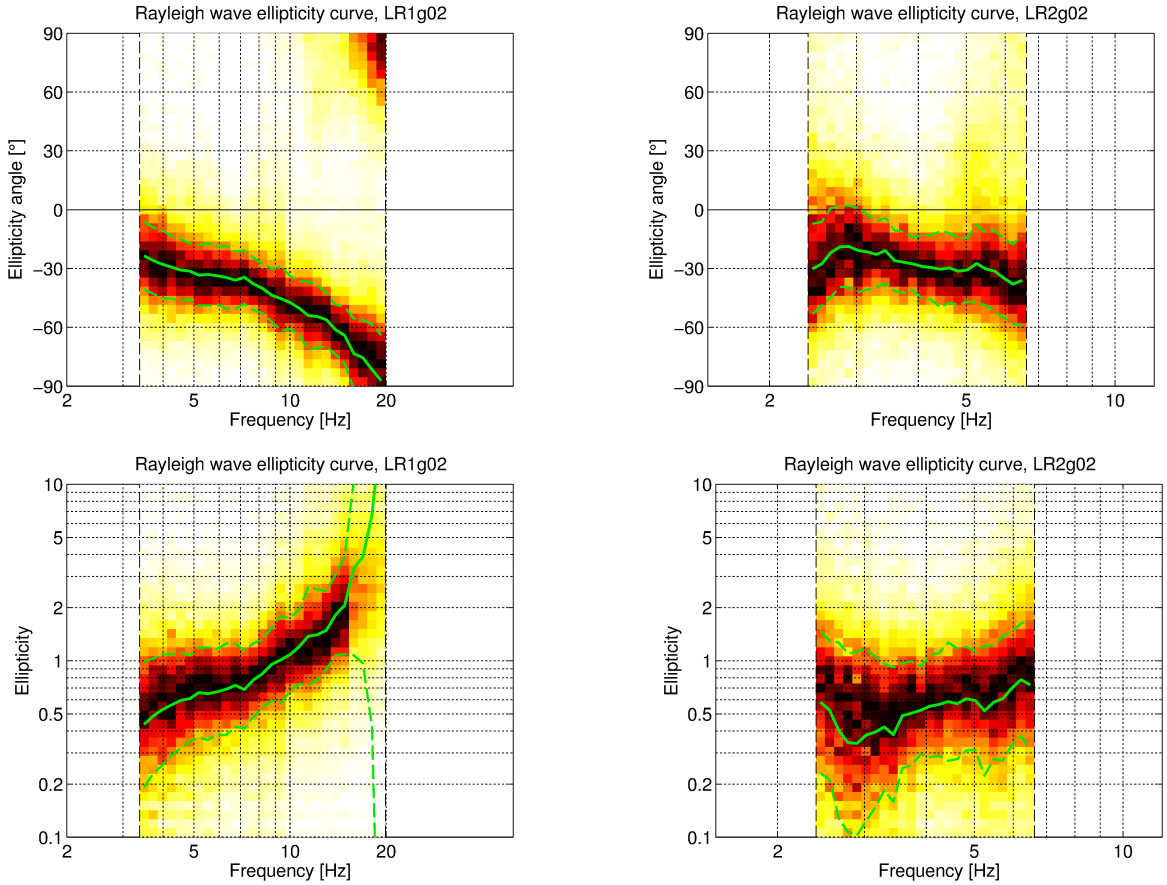


Figure 9: Rayleigh wave ellipticity curves obtained with the WaveDec technique (Maranò et al., 2012). Top line: Rayleigh wave ellipticity angles obtained using array 1 (left) and array 2 (right). Bottom line: Rayleigh wave ellipticity curve, i.e. the absolute value of the tangent of the ellipticity angle, for the curve of array 1 (left) and array 2 (right).

## 3.6 SPAC

The SPAC (Aki, 1957) curves of the vertical components have been calculated using the M-SPAC (Bettig et al., 2001) technique implemented in geopsy. Rings with different radius ranges had been defined previously and for all station pairs with distance inside this radius range, the cross-correlation was calculated in different frequency ranges. These cross-correlation curves are averaged for all station pairs of the respective ring and give the SPAC curves. The rings are defined in such a way that at least three station pairs contribute and that their connecting vectors have a good directional coverage.
The SPAC curves for all defined rings are shown in Fig. 10 for array 1 and Fig. 11 for array 2. The black points indicate the data values which contributed to the final dispersion curve estimation, which was made with the function `spac2disp` of the geopsy package. These resulting dispersion curves are shown in Fig. 12.
Using SPAC, we can retrieve a Rayleigh wave dispersion curve between 1.8 and 16.8 Hz for array 1 and between 1.8 and 8.8 Hz for array 2.

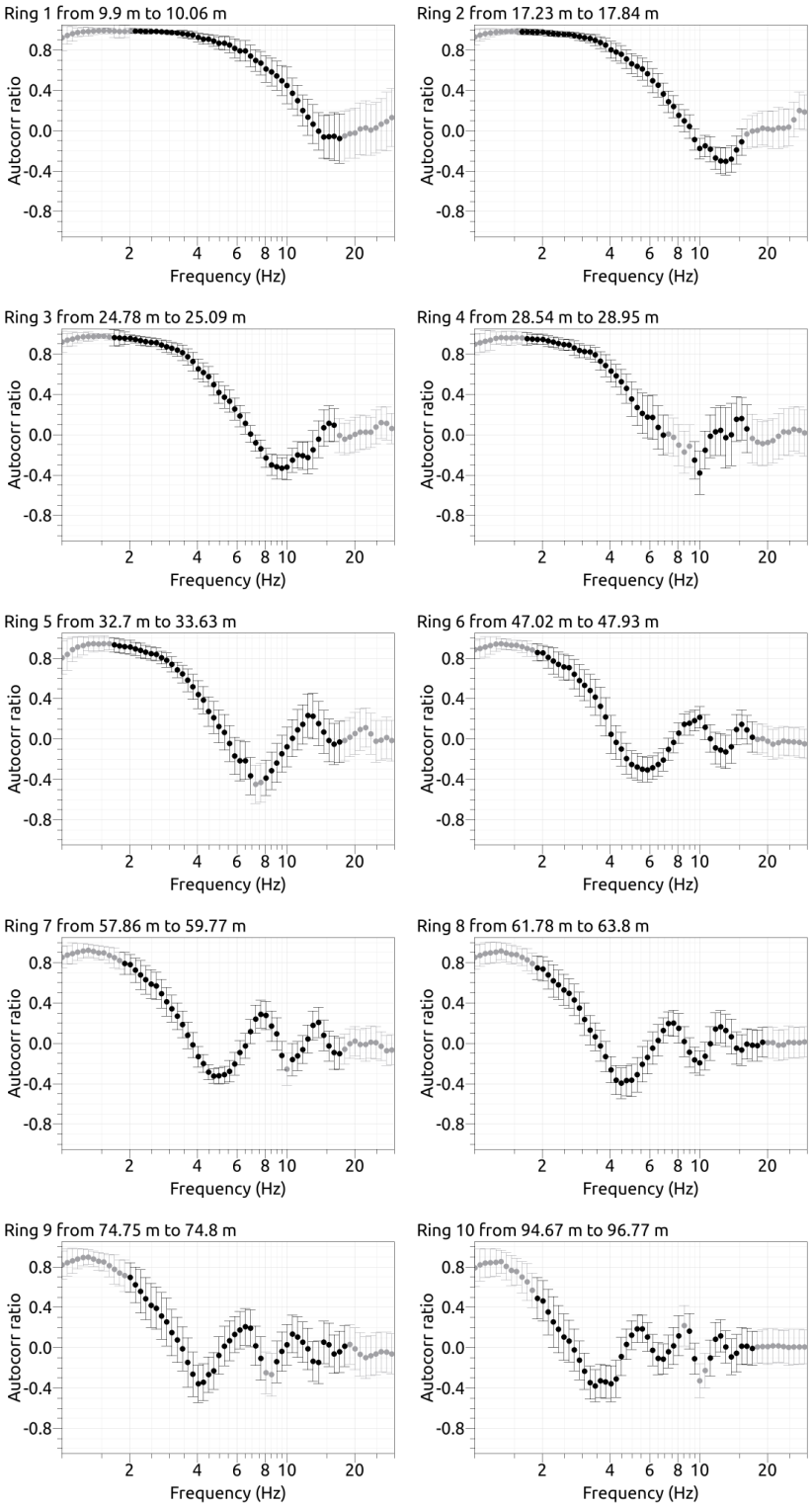


Figure 10: SPAC curves for array 1. The black data points contributed to the dispersion curve estimation.

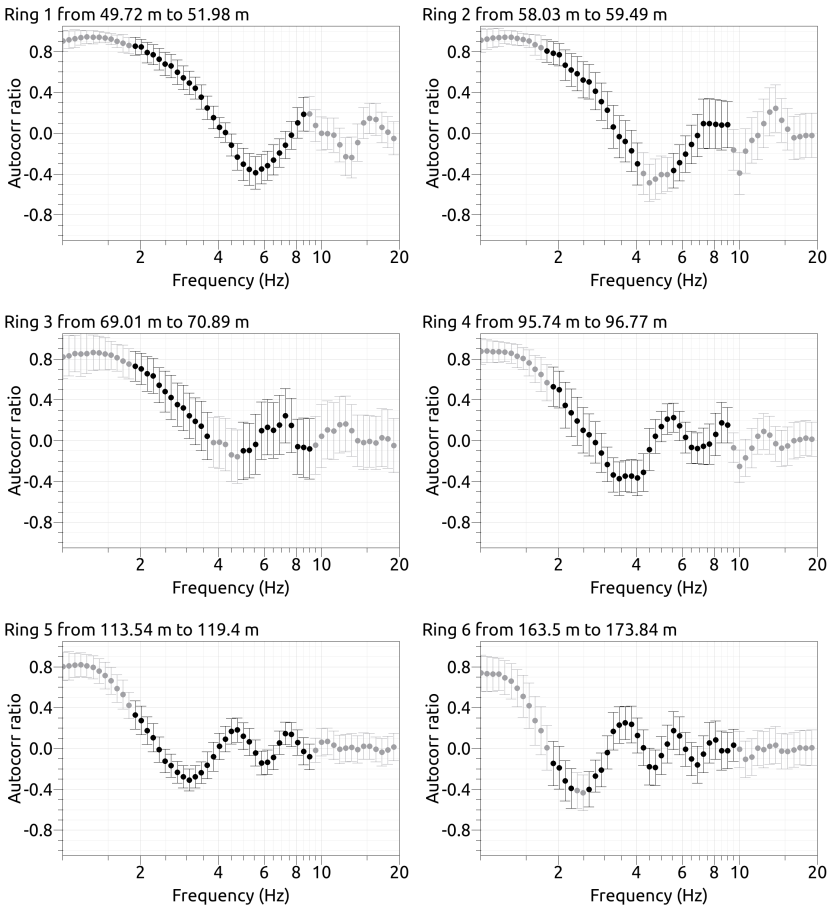


Figure 11: SPAC curves for array 2. The black data points contributed to the dispersion curve estimation.

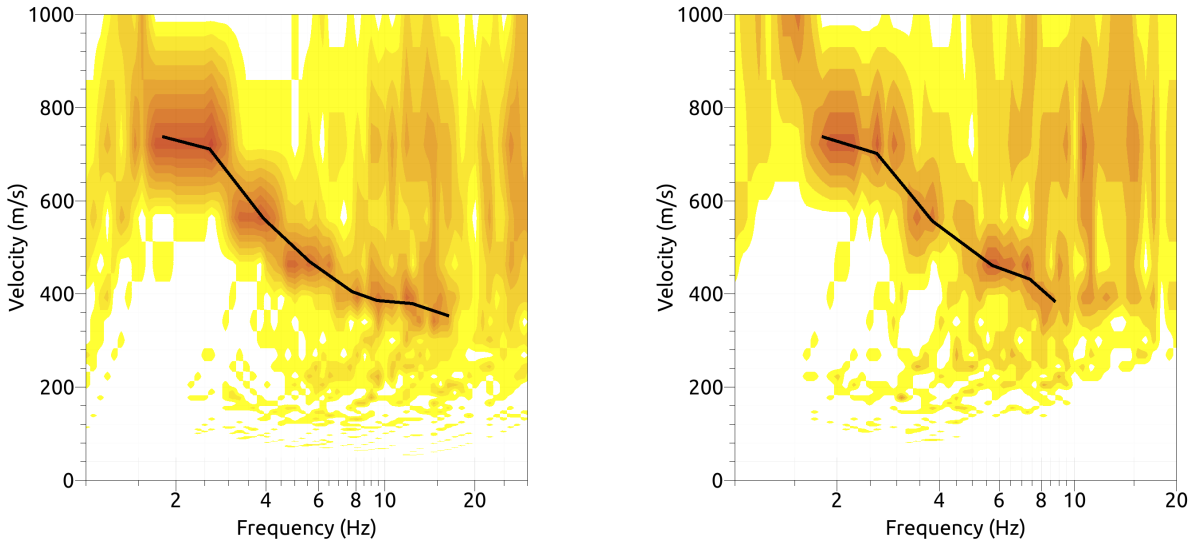


Figure 12: Resulting Rayleigh wave velocities for array 1 (left) and array 2 (right). The black line corresponds to the picked dispersion curve.

## 3.7 Summary

Fig. 13 gives an overview of the dispersion and ellipticity curves determined by the different methods.
For Love waves, the HRFK and WaveDec results for the respective arrays are in good agreement and we can identify a continuous dispersion curve between 2.0 and 22.0 Hz. Between 4 and 8 Hz, however, the different curves diverge more than in the other frequency ranges.
For the Rayleigh waves, there is a very good agreement between the different methods, except for the HRFK curves for the radial component, which show higher velocities at the low-frequency array resolution limits of the respective arrays. The dispersion curves measured with SPAC and HRFK diverge around 2 Hz.
The ellipticity curves retrieved using the different methods are in good qualitative agreement. The single-station ellipticity curve determined with RayDec is the only one to cover frequencies lower than 2 Hz. Above, the WaveDec curve from array 2 shows a more pronounced trough around 3 Hz. The WaveDec curve of array 1 shows some signs for a singularity at around 20 Hz, and retrograde particle motion below. If the singularity is real, it would correspond to a strong velocity contrast in the very shallow structure. The retrograde particle motion at lower frequencies, especially around the trough at 3 Hz, indicates that there is no strong velocity contrast in the deeper part of the structure. Therefore, we interpret the peak below 1 Hz as a non-singular one.

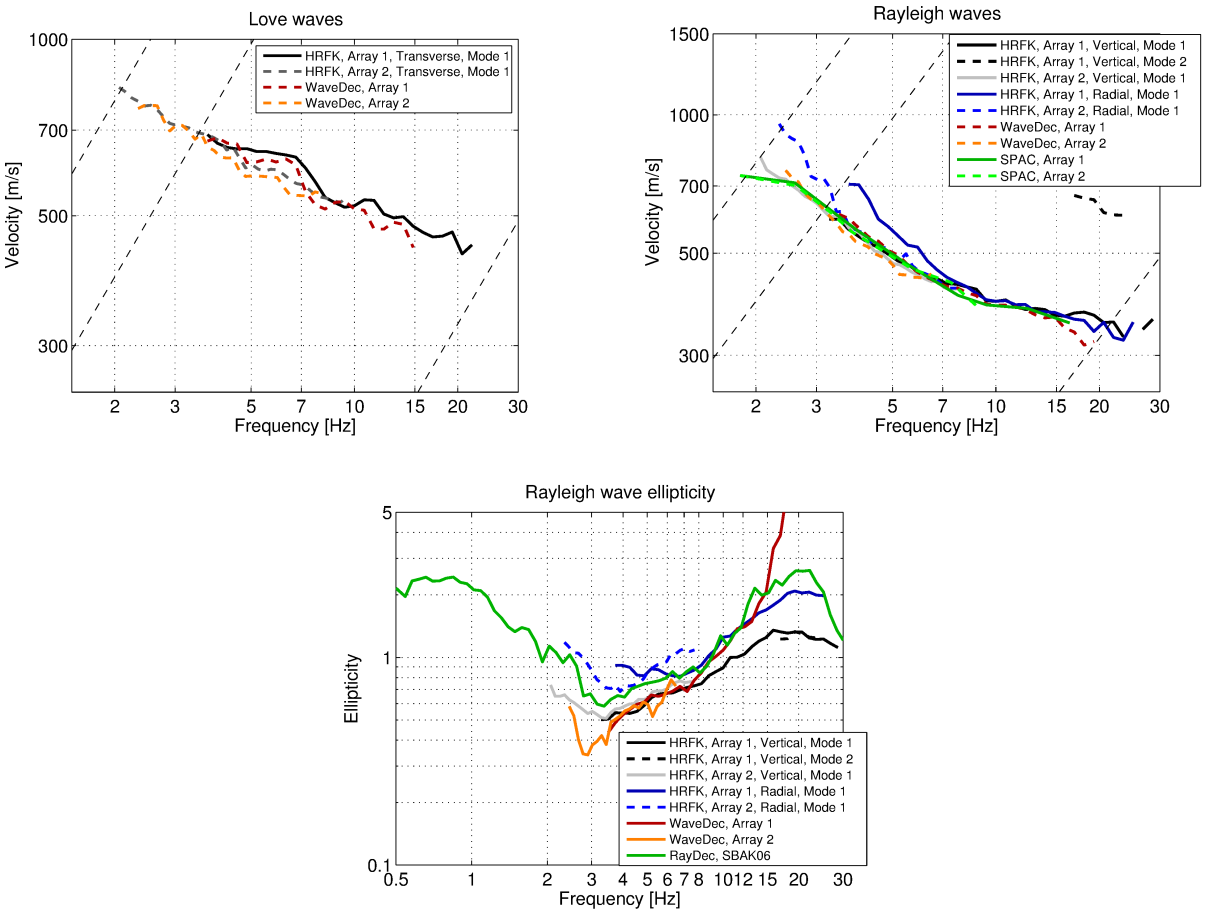


Figure 13: Overview of the Love and Rayleigh wave dispersion curves as well as the ellipticity curves for both arrays. The dashed lines indicate the theoretical resolution limits of the array. The RayDec ellipticity curve corresponds to station SBAK43.

# 4 Data inversion

## 4.1 Inversion parameterization

For the inversion, six different parameterizations have been used in total. The first five had free values of the depths and velocities of the different layers, ranging from four to eight layers (including half-space). The last parameterization had fixed layer depths and consisted of 19 layers in total. The P-wave velocities were allowed to vary up to 5000 m/s. The S-wave velocities were allowed to range from 50 to 3500 m/s. The deepest layers were parameterized to range to a depth of maximum 1000 m. The density was fixed to $2\,300\,kg/m^3$ for the lowest layer and to $2\,000\,kg/m^3$ for all other layers. In general, no low-velocity zones were allowed.

## 4.2 Inversion targets

We performed inversions using different parts of the measured curves as inversion targets. A first try was using both the Rayleigh and Love wave dispersion curves measured with HRFK, assuming that they correspond to the respective fundamental modes, and only the peak of the ellipticity curve measured by RayDec as ellipticity target, following the recommendations of Hobiger et al. (2013) for ellipticity curves without singularities. An example of such an inversion is shown in Fig. 15 for an inversion with seven layers. For all of these inversions, the Love wave dispersion curve is not well fitted, even if the Rayleigh wave dispersion curve and especially the ellipticity curve are well fitted, resulting in relatively high misfit values (see 3). The measured Love wave dispersion curve shows higher velocities than the Rayleigh wave dispersion curve, similar to observations at other locations in Basel. It is not easy to fit the data using a model without low-velocity zones in that case.
Another test was performed assuming that the Love wave dispersion curve belongs to the first higher mode, but without success. Allowing for low-velocity layers, it was actually possible to get a slightly better fit of the data, but the resulting models were not very realistic. Therefore we decided to neglect the Love wave dispersion curve for the final reference inversions and only use the Rayleigh wave dispersion curve, together with the RayDec ellipticity curve and including the WaveDec ellipticity curve from array 2. The details of the inversion targets are indicated in Table 2 and the corresponding curves are shown in Fig. 14.

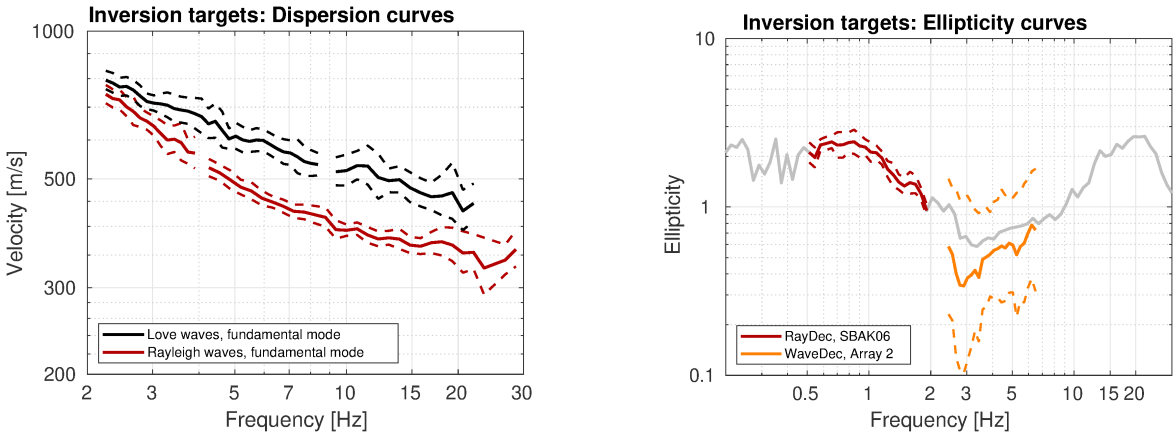


Figure 14: Overview of the dispersion (left) and ellipticity (right) curves used as targets for the different inversions.

Table 2: List of the different data curves used as target in the different inversions. The Love wave dispersion curves were not used in the final reference inversions.

| Array | Method | Wave type | Mode | Curve type | Frequency range [Hz] |
|---|---|---|---|---|---|
| 1 | HRFK (T) | Love | fundamental | dispersion | 9.2 - 21.5 |
| 2 | HRFK (T) | Love | fundamental | dispersion | 2.3 - 8.4 |
| 1 | HRFK (V) | Rayleigh | fundamental | dispersion | 4.3 - 28.5 |
| 2 | HRFK (V) | Rayleigh | fundamental | dispersion | 2.3 - 4.0 |
| | RayDec (SBAK06) | Rayleigh | fundamental | ellipticity | 0.50 - 1.86 |
| 2 | WaveDec | Rayleigh | fundamental | ellipticity | 2.44 - 6.49 |

## 4.3 Inversion results

We performed six inversions with different parameterizations for the different targets. In Table 3, the obtained minimum misfit values for the inversions using both Love and Rayleigh wave dispersion curves as fundamental modes (SBAK4l-SBAKfix) are shown together with the inversions without the Love wave dispersion curve, the reference inversions (SBAK4lR-SBAKfixR). Each inversion run produced 500 000 total models in order to assure a good convergence of the solution. For the first target, only the resulting figures for SBAK7l are shown in Fig. 15. The results of the inversions SBAK4lR to SBAKfixR are shown in Figs 16 - 21.
For the reference inversions, SBAK4lR produces a minimum misfit value which is much larger than the ones of the other inversions, indicating that four layers are not enough to fit the data. The other inversions yield similar misfit values and fit the data in a comparable way. Using the fixed layer approach, the minimum misfit was also a bit higher. This is probably because the interface depths were fixed at non-optimum depths.

Table 3: List of inversions

| Inversion | Number of layers | Number of models | Minimum misfit |
|---|---|---|---|
| SBAK4l | 4 | 500 000 | 1.129 |
| SBAK5l | 5 | 500 000 | 1.075 |
| SBAK6l | 6 | 500 000 | 0.939 |
| SBAK7l | 7 | 500 000 | 1.048 |
| SBAK8l | 8 | 500 000 | 1.342 |
| SBAKfix | 19 | 500 000 | 1.426 |
| SBAK4lR | 4 | 500 000 | 0.515 |
| SBAK5lR | 5 | 500 000 | 0.309 |
| SBAK6lR | 6 | 500 000 | 0.322 |
| SBAK7lR | 7 | 500 000 | 0.300 |
| SBAK8lR | 8 | 500 000 | 0.349 |
| SBAKfixR | 19 | 500 000 | 0.380 |

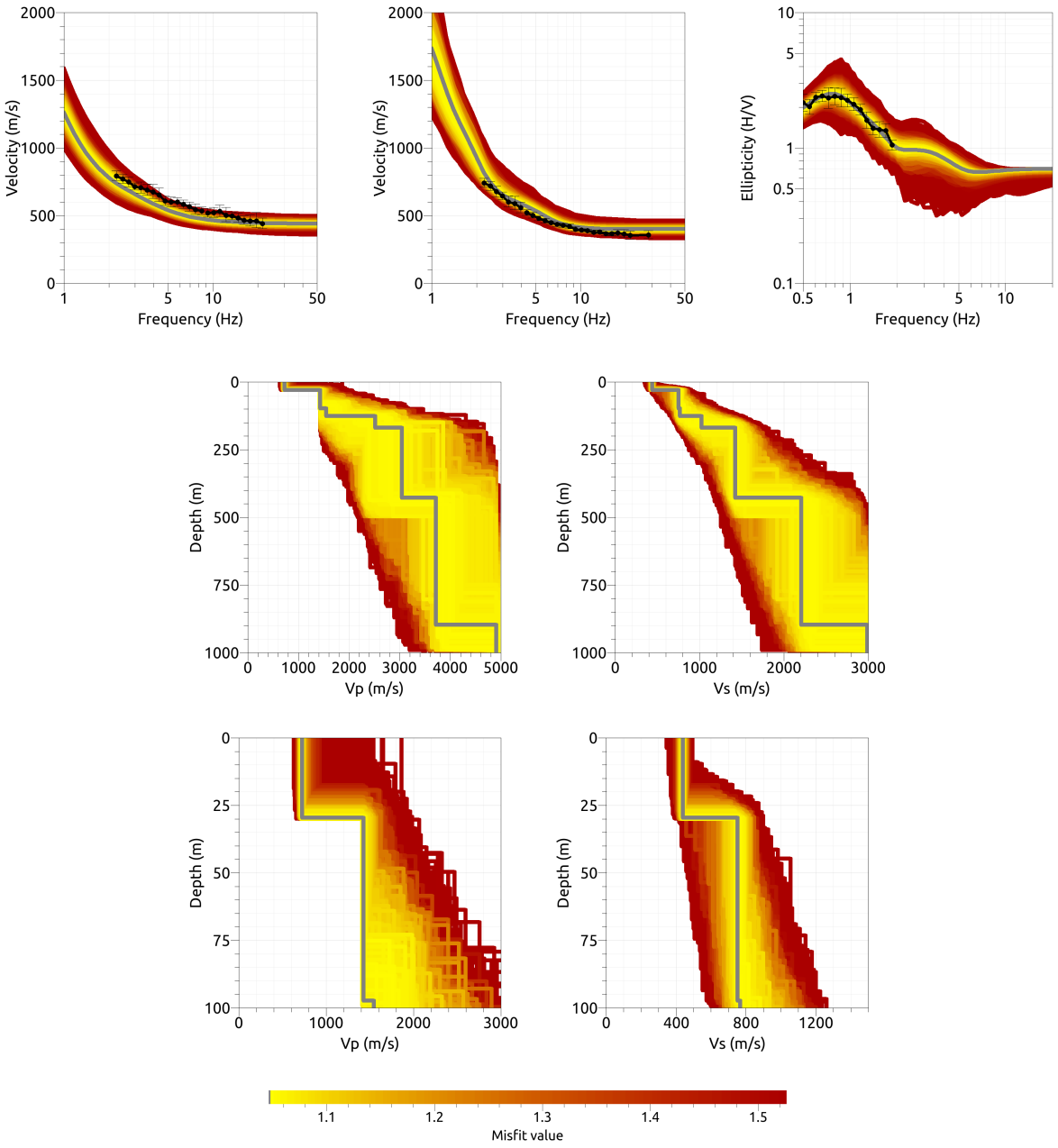


Figure 15: Inversion SBAK7l. Top line: Dispersion curves for the Love wave fundamental mode (left) and the Rayleigh wave fundamental mode (center) and ellipticity curves of the Rayleigh wave fundamental mode (right). Center line: P-wave velocity profiles (left) and S-wave velocity profiles (right). Bottom line: Zoom on the upper 100 m of the P-wave (left) and S-wave (right) velocity profiles. The black dots indicate the data points used for the inversion, the gray line indicates the best-fitting model.

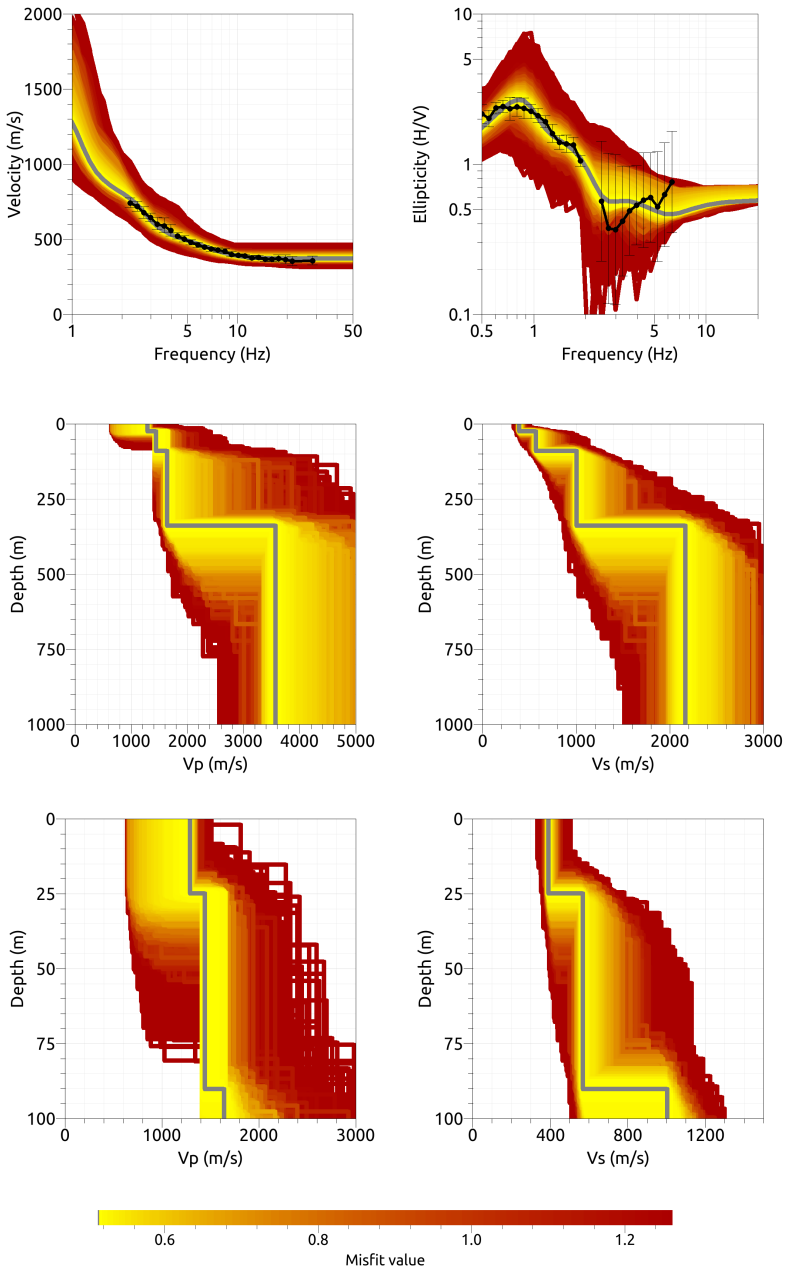


Figure 16: Inversion SBAK4lR. Top line: Dispersion curves (left) and ellipticity curves (right) of the Rayleigh wave fundamental mode. Center line: P-wave velocity profiles (left) and S-wave velocity profiles (right). Bottom line: Zoom on the upper 100 m of the P-wave (left) and S-wave (right) velocity profiles. The black dots indicate the data points used for the inversion, the gray line indicates the best-fitting model.

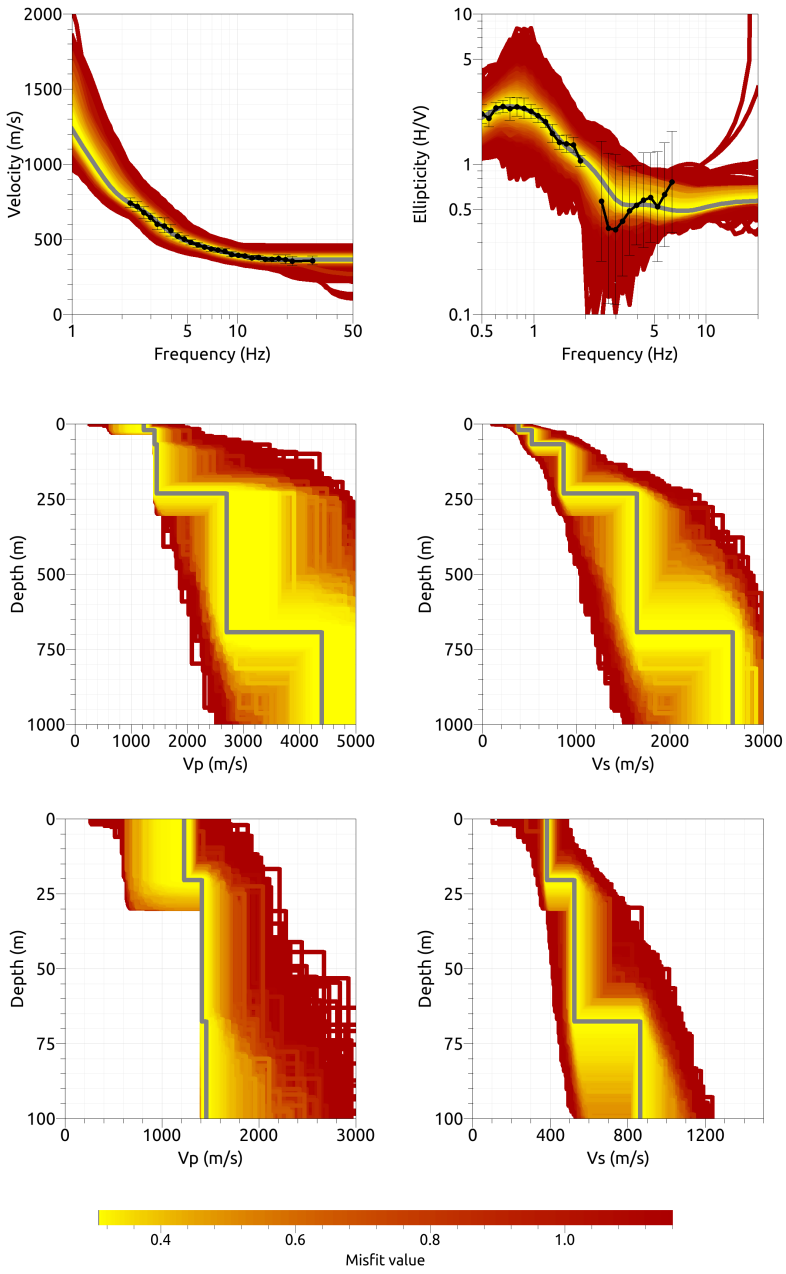


Figure 17: Inversion SBAK5lR. Top line: Dispersion curves (left) and ellipticity curves (right) of the Rayleigh wave fundamental mode. Center line: P-wave velocity profiles (left) and S-wave velocity profiles (right). Bottom line: Zoom on the upper 100 m of the P-wave (left) and S-wave (right) velocity profiles. The black dots indicate the data points used for the inversion, the gray line indicates the best-fitting model.

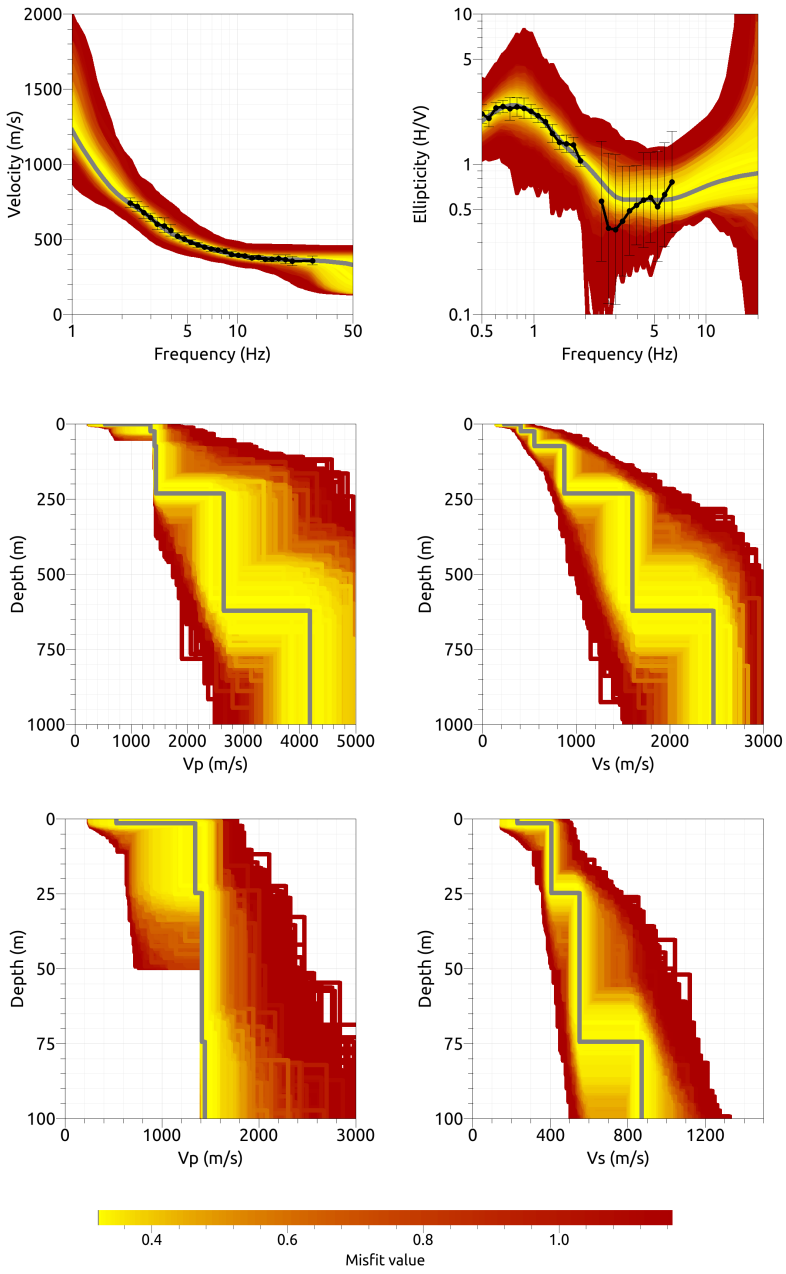


Figure 18: Inversion SBAK6lR. Top line: Dispersion curves (left) and ellipticity curves (right) of the Rayleigh wave fundamental mode. Center line: P-wave velocity profiles (left) and S-wave velocity profiles (right). Bottom line: Zoom on the upper 100 m of the P-wave (left) and S-wave (right) velocity profiles. The black dots indicate the data points used for the inversion, the gray line indicates the best-fitting model.

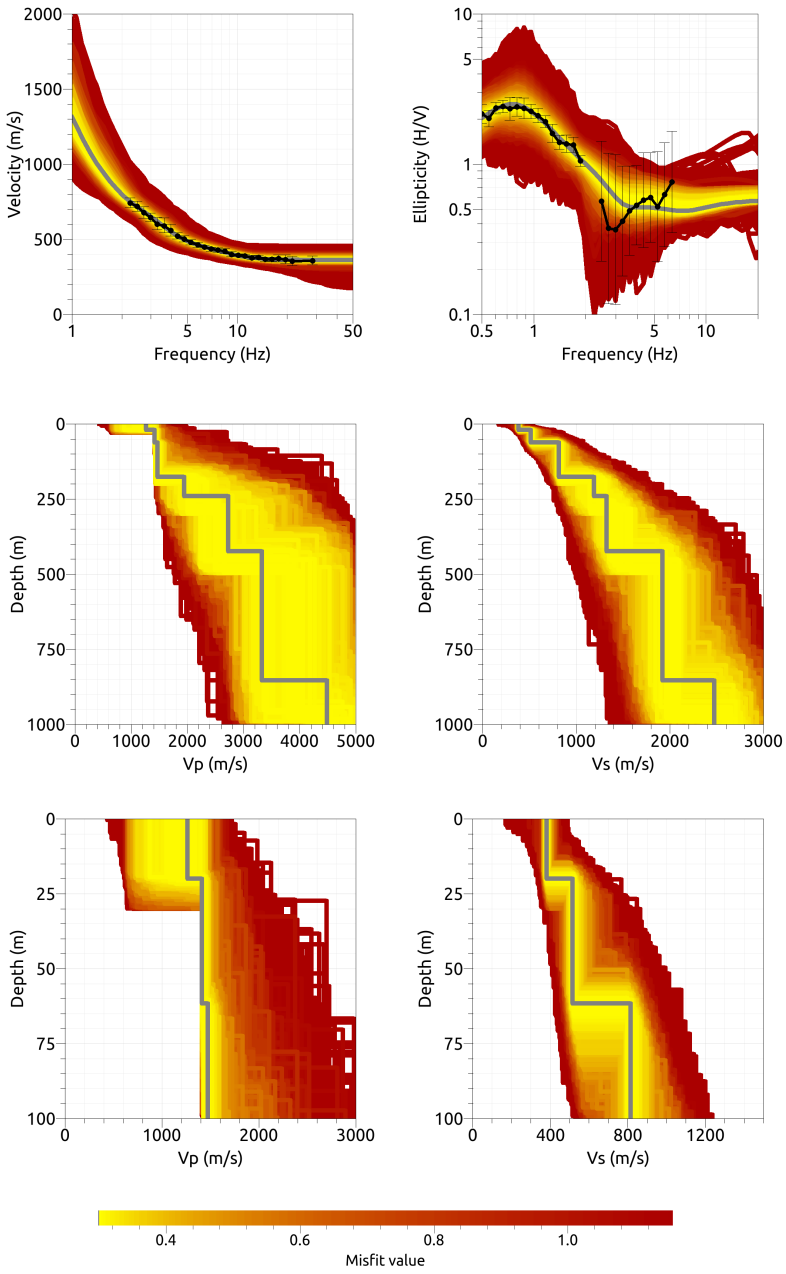


Figure 19: Inversion SBAK7lR. Top line: Dispersion curves (left) and ellipticity curves (right) of the Rayleigh wave fundamental mode. Center line: P-wave velocity profiles (left) and S-wave velocity profiles (right). Bottom line: Zoom on the upper 100 m of the P-wave (left) and S-wave (right) velocity profiles. The black dots indicate the data points used for the inversion, the gray line indicates the best-fitting model.

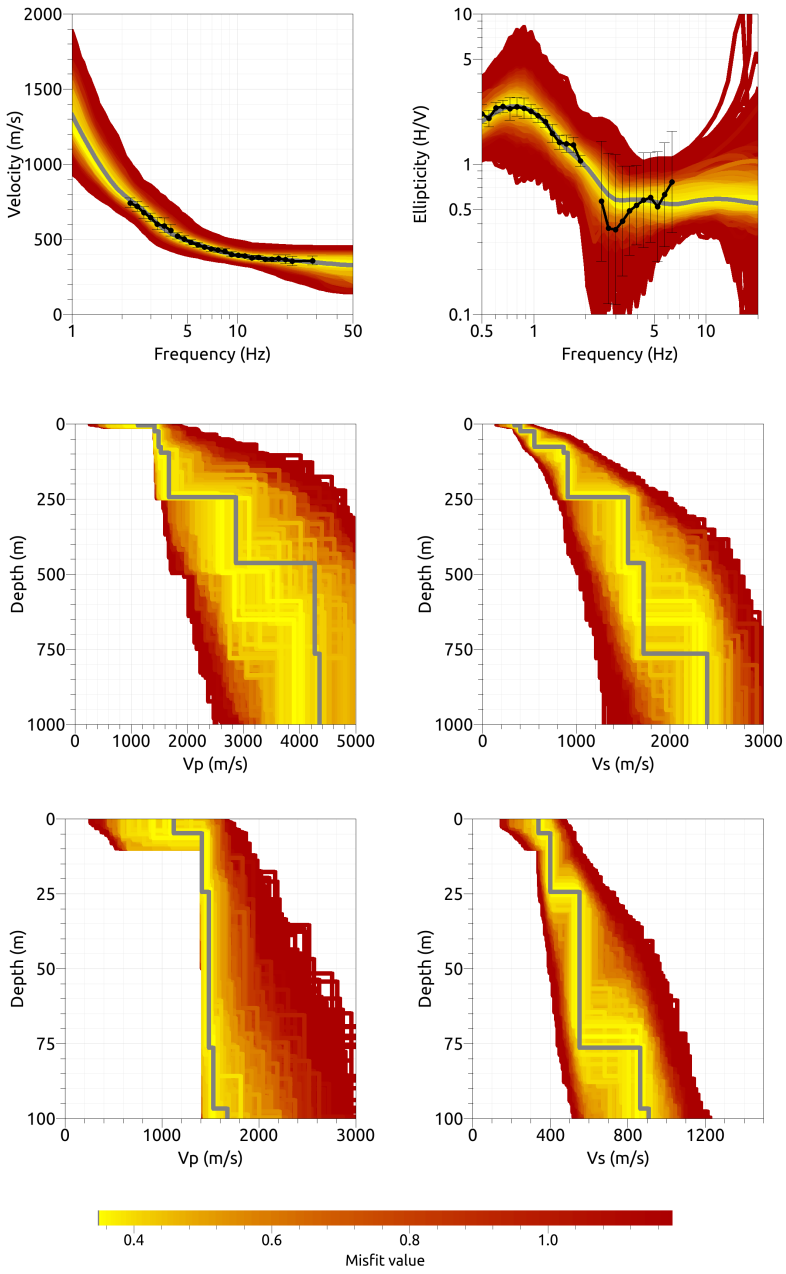


Figure 20: Inversion SBAK8lR. Top line: Dispersion curves (left) and ellipticity curves (right) of the Rayleigh wave fundamental mode. Center line: P-wave velocity profiles (left) and S-wave velocity profiles (right). Bottom line: Zoom on the upper 100 m of the P-wave (left) and S-wave (right) velocity profiles. The black dots indicate the data points used for the inversion, the gray line indicates the best-fitting model.

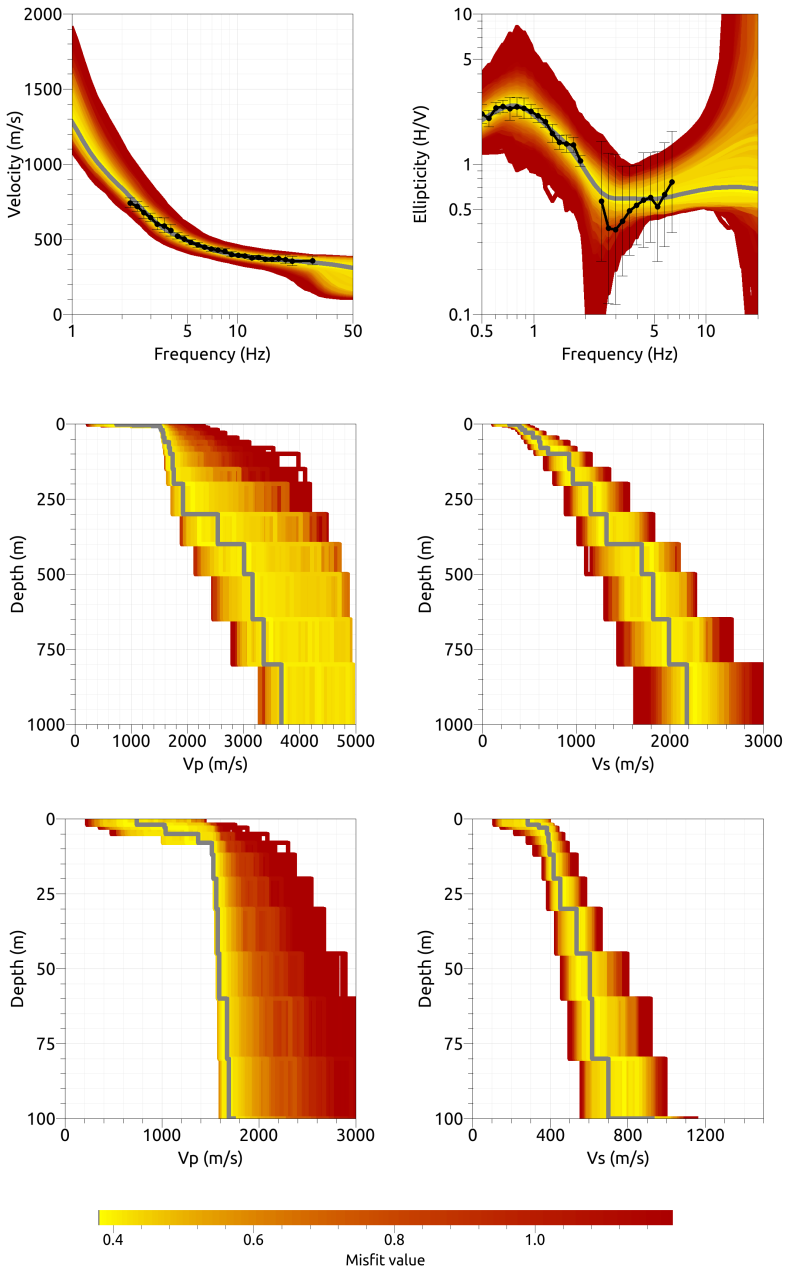


Figure 21: Inversion SBAKfixR. Top line: Dispersion curves (left) and ellipticity curves (right) of the Rayleigh wave fundamental mode. Center line: P-wave velocity profiles (left) and S-wave velocity profiles (right). Bottom line: Zoom on the upper 100 m of the P-wave (left) and S-wave (right) velocity profiles. The black dots indicate the data points used for the inversion, the gray line indicates the best-fitting model.

## 4.4 Overview of the inversion result

The best-fitting models of the inversions SBAK4lR-SBAKfixR are shown in Fig. 22. Neglecting SBAK4l, the models are similar. The more complex parameterizations show small superficial layers of lower velocities, but all models show shear-wave velocities of around 400 m/s down to about 20-25 m, where the velocity increases to about 520-550 m/s. Another contrast is found at 60 to 80 m of depth, where the velocity increases to about 860 m/s. At a depth of about 230 m, the velocity increases to around 1600 m/s. For the fixed-depth approach, the velocity increases more gradually.
The $V_{S30}$ value for the inversions ranges from 404.8 to 419.5 m/s (average value 412.4 $\pm$ 6.4 $m/s$). This corresponds to soil class B in EC8 and C in SIA261.

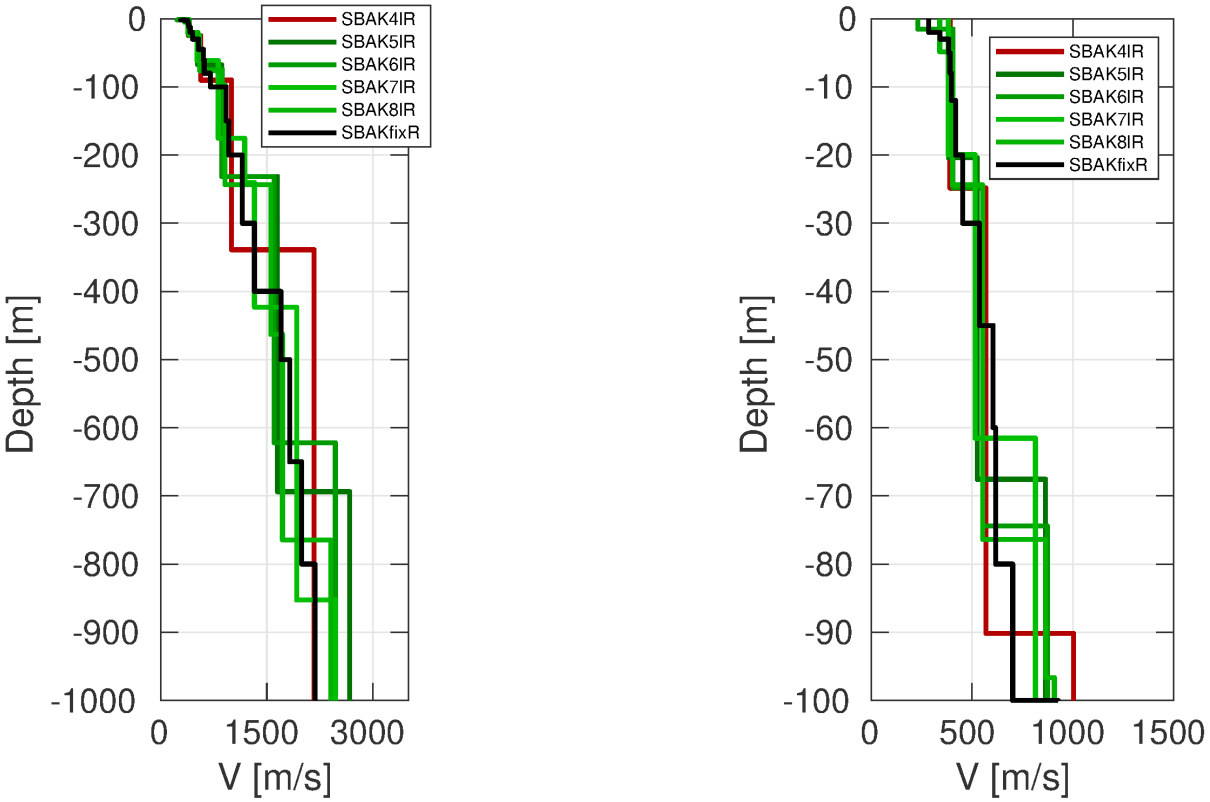


Figure 22: Overview of shear-wave velocity profiles of the best-fitting models of all inversions (left) and a zoom on the shallow part (right).

## 4.5 SH transfer function

In Fig. 23, the theoretical shear-wave transfer function for the best models resulting from the inversions is compared with the empirical amplification. The empirical amplification for station SBAK is based on 10 events so far. The empirical amplification shows a relatively high level of amplification over the whole frequency range, with a first peak at around 0.7 Hz and another peak at around 2 Hz. The curve for the inversion models in this frequency range is shifted towards lower amplifications. This can be explained by edge-generated surface waves, which cannot be modeled using the 1-dimensional SH resonance. At frequencies between 5 and 20 Hz, the empirical amplification shows some very pronounced peaks which might be explained by the very shallow substructure, which has not been resolved in enough detail using the passive methods.

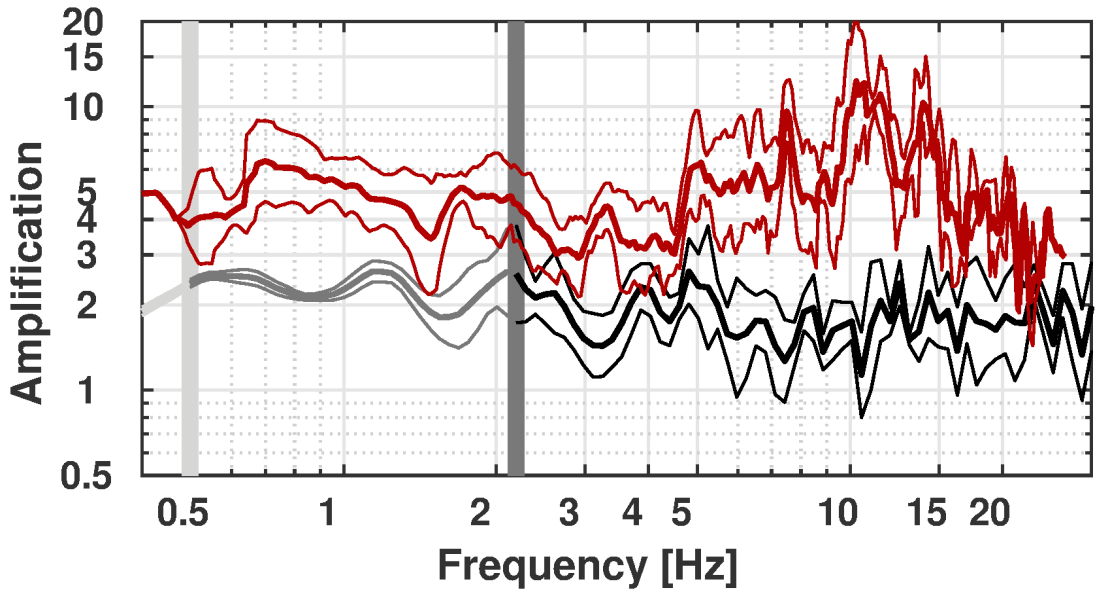


Figure 23: Comparison between the modeled amplification for the final set of best models of the different inversions (SBAK5lR-SBAKfixR; in grey to black, with standard deviation) and the empirical amplification measured at station SBAK (red, with standard deviation). The vertical light and dark grey bars correspond to the lowest frequency of the ellipticity and dispersion curves, respectively.

## 4.6 Quarter-wavelength representation

The quarter-wavelength velocity approach (Joyner et al., 1981) provides, for a given frequency, the average velocity at a depth corresponding to 1/4 of the wavelength of interest. It is useful to identify the frequency limits of the experimental data (the minimum frequency of the dispersion curve used in the inversion is 2.3 Hz, the minimum frequency used for the ellipticity inversion 0.5 Hz). The results using this proxy show that the dispersion curves constrain the profiles down to less than 100 m, but the ellipticity information down to more than 400 m (Fig. 24). Moreover, the quarter wavelength impedance-contrast introduced by Poggi et al. (2012) is also displayed in the figure. It corresponds to the ratio between two quarter-wavelength average velocities, respectively from the top and the bottom part of the velocity profile, at a given frequency (Poggi et al., 2012). This curve shows a strong contrast at the fundamental frequency of the site.

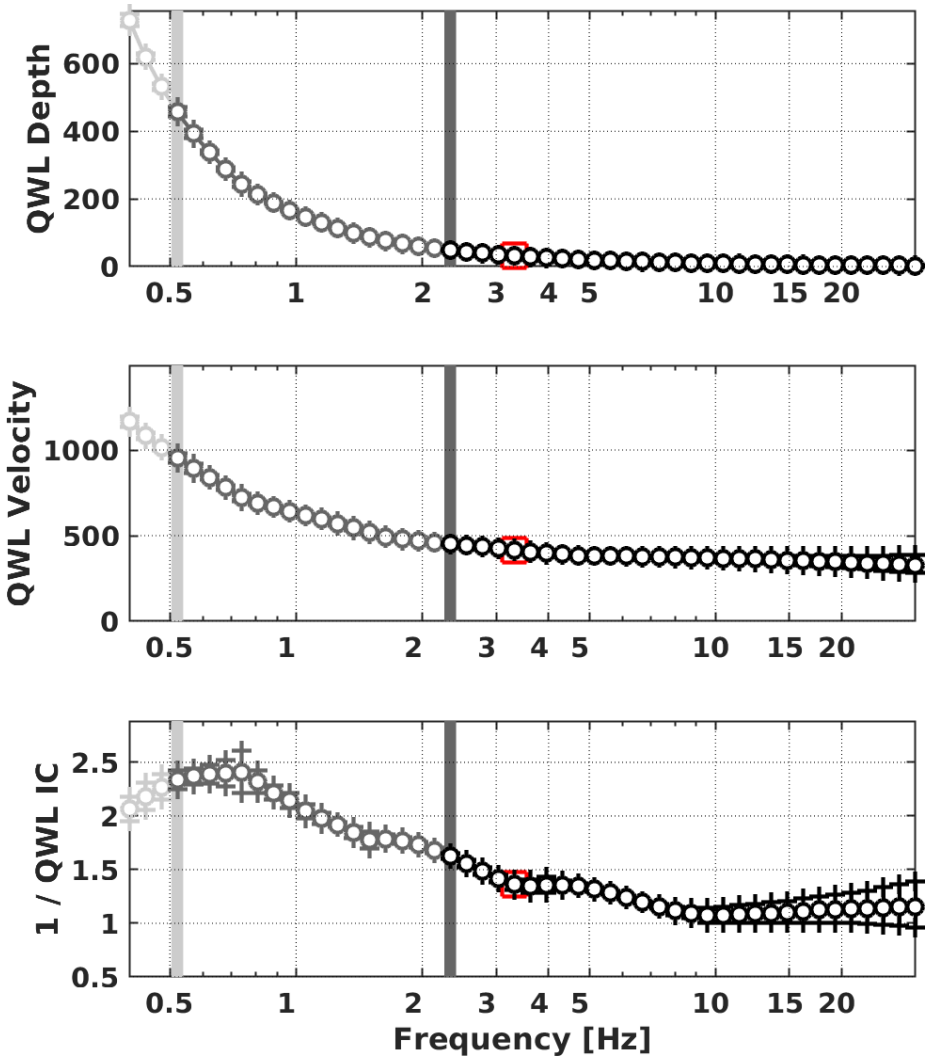


Figure 24: Quarter wavelength representation of the velocity profile for the best models of the inversions (top: depth, center: velocity, bottom: inverse of the impedance contrast). The black curves are constrained by the dispersion curves, the light grey curves are not constrained by the data. The red square corresponds to $V_{S30}$.

# 5 Conclusion

We performed a passive array measurement with two arrays to characterize the soil underneath station SBAK in Basel-Klybeck (BS), located on alluvial deposits of the Rhine valley.
The dispersion curves for Love and Rayleigh waves could be measured over a wide frequency range, from around 2 to over 20 Hz for both Love and Rayleigh waves. The ellipticity peak frequency was measured at around 0.7 Hz. The ellipticity peak does not correspond to a singularity.
Similar to other places in Basel, it was not possible to successfully invert Love and Rayleigh waves together and the Love waves were therefore neglected in the inversion. The joint inversion of Rayleigh wave dispersion and ellipticity curves showed that the structure can be explained by models with interfaces at around 20-25 m, 60-80 m and 230 m depth. The $V_{S30}$ of the best models is about 412 m/s, corresponding to soil class B in EC8 and C in SIA261.

# Acknowledgements

The authors thank Elisabeth Rauchegger and Ulrich Aerne for their help during the array measurements.

# References


Aki, K. (1957). Space and time spectra of stationary stochastic waves, with special reference to microtremors. *Bull. Earthquake Res. Inst. Tokyo Univ.*, 35:415–456.

Bettig, B., Bard, P.-Y., Scherbaum, F., Riepl, J., Cotton, F., Cornou, C., and Hatzfeld, D. (2001). Analysis of dense array noise measurements using the modified spatial auto-correlation method (SPAC): application to the Grenoble area. *Boll. Geof. Teor. Appl.*, 42:281–304.

Burjánek, J., Gassner-Stamm, G., Poggi, V., Moore, J. R., and Fäh, D. (2010). Ambient vibration analysis of an unstable mountain slope. *Geophys. J. Int.*, 180:820–828.

Burjánek, J., Moore, J. R., Molina, F. X. Y., and Fäh, D. (2012). Instrumental evidence of normal mode rock slope vibration. *Geophys. J. Int.*, 188:559–569.

Fäh, D., Wathelet, M., Kristekova, M., Havenith, H., Endrun, B., Stamm, G., Poggi, V., Burjanek, J., and Cornou, C. (2009). Using ellipticity information for site characterisation. NERIES deliverable JRA4 D4, available at http://www.neries-eu.org.

Hobiger, M., Bard, P.-Y., Cornou, C., and Le Bihan, N. (2009). Single station determination of Rayleigh wave ellipticity by using the random decrement technique (RayDec). *Geophys. Res. Lett.*, 36.

Hobiger, M., Cornou, C., Wathelet, M., Di Giulio, G., Knapmeyer-Endrun, B., Renalier, F., Bard, P.-Y., Savvaidis, A., Hailemikael, S., Le Bihan, N., Ohrnberger, M., and Theodoulidis, N. (2013). Ground structure imaging by inversions of Rayleigh wave ellipticity: Sensitivity analysis and application to European strong motion sites. *Geophys. J. Int.*, 192:201–229.

Joyner, W. B., Warrick, R. E., and Fumal, T. E. (1981). The effect of Quaternary alluvium on strong ground motion in the Coyote Lake, California, earthquake of 1979. *Bull. Seismol. Soc. Am.*, 71(4):1333–1349.

Maranò, S., Reller, C., Loeliger, H.-A., and Fäh, D. (2012). Seismic waves estimation and wavefield decomposition: Application to ambient vibrations. *Geophys. J. Int.*, 191:175–188.

Poggi, V., Edwards, B., and Fäh, D. (2012). Characterizing the Vertical-to-Horizontal ratio of ground motion at soft-sediment sites. *Bull. Seismol. Soc. Am.*, 102(6):2741–2756.

Poggi, V. and Fäh, D. (2010). Estimating Rayleigh wave particle motion from three-component array analysis of ambient vibrations. *Geophys. J. Int.*, 180:251–267.